Inorganic Chemistry

Article

pubs.acs.org/IC

Phase Relationships in the $BaO-Ga_2O_3-Ta_2O_5$ System and the Structure of $Ba_6Ga_{21}TaO_{40}$

Jiang Cao, Xiaodi Yu, Xiaojun Kuang,* and Qiang Su

MOE Key Laboratory of Bioinorganic and Synthetic Chemistry, State Key Laboratory of Optoelectronic Materials and Technologies, KLGHEI of Environment and Energy Chemistry, School of Chemistry and Chemical Engineering, Sun Yat-Sen University, Guangzhou 510275, P. R. China

Supporting Information

ABSTRACT: Phase relationships in the $BaO-Ga_2O_3-Ta_2O_5$ ternary system at 1200 °C were determined. The $A_6B_{10}O_{30}$ tetragonal tungsten bronze (TTB) related solution in the $BaO-Ta_2O_5$ subsystem dissolved up to ~11 mol % Ga_2O_3, forming a ternary trapezoid-shaped TTB-related solid solution region defined by the $BaTa_2O_6$, $Ba_{1.1}Ta_5O_{13.6}$, $Ba_{1.58}Ga_{0.92}Ta_{4.08}O_{13.16}$, and $Ba_6GaTa_9O_{30}$ compositions in the $BaO-Ga_2O_3-Ta_2O_5$ system. Two ternary phases $Ba_6Ga_{21}TaO_{40}$ and eight-layer twinned hexagonal perovskite solid solution $Ba_8Ga_{4-x}Ta_{4+0.6x}O_{24}$ were confirmed in the $BaO-Ga_2O_3-Ta_2O_5$ system. $Ba_6Ga_{21}TaO_{40}$ crystallized in a monoclinic cell of a = 15.9130(2) Å, b = 11.7309(1) Å, c = 5.13593(6) Å, β = 107.7893(9)°, and Z = 1 in space group $C2/m$. The structure of $Ba_6Ga_{21}TaO_{40}$ was solved by the charge flipping method, and it represents a three-dimensional (3D) mixed GaO_4 tetrahedral and GaO_6/TaO_6 octahedral framework, forming mixed 1D 5/6-fold tunnels that accommodate the Ba cations along the c axis. The electrical property of $Ba_6Ga_{21}TaO_{40}$ was characterized by using ac impedance spectroscopy.

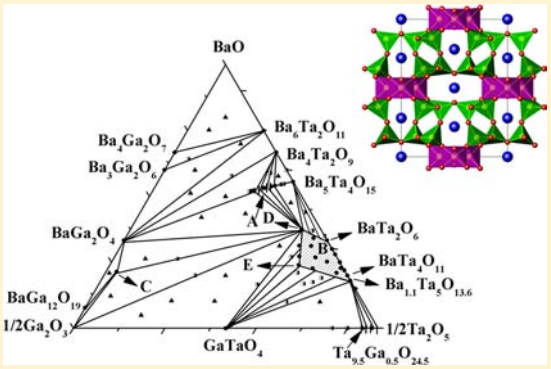

1. INTRODUCTION

Titanates, niobates, and tantalates have been widely investigated as important dielectric oxide materials.[1,2] Although the cost of tantalum is higher than those of niobium and titanium,[3] 2:1 ordered complex perovskite tantalates are attractive as microwave dielectric ceramic materials owing to their superior microwave dielectric performance.[1,4,5] For example, the commercially available resonators $Ba_3ZnTa_2O_9$ and $Ba_3MgTa_2O_9$ exhibit a permittivity of ~30, high quality factors ($Q \times f \geq$ 150 000 GHz, where Q is the quality factor, inverse dielectric loss, and f is the resonant frequency), and zero temperature coefficients of resonant frequency τ_f.[1] Hexagonal perovskites tantalates also display fascinating microwave dielectric properties such as eight-layer twinned hexagonal perovskite $Ba_8MTa_6O_{24}$ (M = Zn, Ni, Co)[5−7], and $Ba_8Li_2Ta_6O_{24}$[8] demonstrated a permittivity of ~30, and high $Q \times f$ values of ~70 000−100 000 GHz, although their high τ_f values within ~25−45 ppm/°C may hinder their application in microwave dielectric resonators. Recently, we isolated an eight-layer twinned B-site deficient hexagonal perovskite $Ba_8Ga_{4-x}Ta_{4+0.6x}O_{24}$ (x = 1.8−3.4; referred to as 8H-BGT) in the $BaO-Ga_2O_3-Ta_2O_5$ ternary system.[9] This 8H-BGT system displayed tunable τ_f from negative to positive over the solid solution limits and improved $Q \times f$ values with B-site deficiency. To our knowledge, the phase relationships in the $BaO-Ga_2O_3-Ta_2O_5$ ternary system have not been determined yet, and only one ternary phase $Ba_6Ga_{21}TaO_{40}$[10] (ICDD PDF 47−0535) has been reported in this system in addition to the 8H-BGT phase. In this study, we report the complete phase relationships in the $BaO-Ga_2O_3-Ta_2O_5$ system at 1200 °C and the crystal structure of the $Ba_6Ga_{21}TaO_{40}$ ternary phase. The $Ba_6Ga_{21}TaO_{40}$ represents a three-dimensional mixed GaO_4 tetrahedral and GaO_6/TaO_6 octahedral network, forming mixed 5/6-fold tunnels that accommodate the Ba cations.

1.1. Review of Subsystems.

The known compounds in the sub-binary systems of the $BaO-Ga_2O_3-Ta_2O_5$ ternary system are summarized in Table 1. The phase equilibria in the $BaO-Ta_2O_5$ binary system were initially studied by Kovba et al.[11] and recently revised by Vanderah et al.[12] in the study of the $BaO-TiO_2-Ta_2O_5$ ternary system from 1275 to 1500 °C. Five line phases, $Ba_6Ta_2O_{11}$, $Ba_4Ta_2O_9$, $Ba_3Ta_2O_8$, $Ba_5Ta_4O_{15}$, and $BaTa_2O_6$, have been reported in the $BaO-Ta_2O_5$ binary system. Kovba et al. observed one cubic and three tetragonal (with slightly different c/a ratio values) phases on $Ba_6Ta_2O_{11}$, and the cubic phase was thought to belong to the double perovskite structure.[13] $Ba_4Ta_2O_9$ adopts hexagonal perovskite related structures, exhibiting three phases classified into a hexagonal $Sr_4Ru_2O_9$-type polymorph and a 6H-$BaTiO_3$ type polymorph with monoclinic and hexagonal modifications.[14] $Ba_3Ta_2O_8$ adopts a monoclinic structure derived from the rhombohedral $Ba_3Nb_2O_8$.[11] $Ba_5Ta_4O_{15}$ is a five-layer B-site

Received: April 21, 2012
Published: June 26, 2012

   dx.doi.org/10.1021/ic3008238 | Inorg. Chem. 2012, 51, 7788−7793

Table 1. Known Compounds in the Sub-Binary Systems of the $BaO-Ga_2O_3-Ta_2O_5$ System

compound	cell parameters	space group	ICDD PDF number
	$BaO-Ta_2O_5$ system		
$Ba_6Ta_2O_{11}$	a = 8.682 Å	$Fm\bar{3}m$[13]	
	a = 6.176 Å, c =8.593 Å	tetragonal	49−0902
$Ba_4Ta_2O_9$	a = 10.2690 Å, c = 8.4729 Å	$P\bar{6}2c$[14]	
	a = 6.1885 Å, c = 16.1277 Å	$P6_3/m$[14]	
	a = 6.1106 Å, b = 16.1109 Å, c = 12.2127 Å, β = 120.332°	$P2_1/c$[14]	
$Ba_5Ta_4O_{15}$	a = 5.776 Å, c = 11.82 Å	$P\bar{3}m1$[15]	72−0631
$BaTa_2O_6$	a = 12.33 Å, b = 10.26 Å, c = 7.67 Å	orthorhombic[16]	20−1046
	a = 12.6 Å, c = 3.95 Å	$P\bar{4}b2$[12,17]	50−1706
	a = 21.116 Å, c = 3.9157 Å	$P6/mmm$[18]	
$Ba_3Ta_2O_8$	a = 10.14 Å, b = 7.449 Å, c = 5.815 Å, γ = 117.43°	$B2/m$[11]	49−0889
$BaTa_4O_{11}$	a = 17.75 Å, c = 3.914 Å	tetragonal[11]	40−0905
$43BaO:57Ta_2O_5$	a = 12.513 Å, c = 3.9296 Å	$P4bm$[12]	
$32.5BaO:67.5Ta_2O_5$	a = 17.695 Å, c = 3.9188 Å	$P4bm$[12]	
$27.5BaO:72.5Ta_2O_5$	a = 12.517 Å, b = 37.482 Å, c = 3.9296 Å	$Pbam$[12]	
	$BaO-Ga_2O_3$ system		
$Ba_4Ga_2O_7$	a = 17.745 Å, b = 10.6719 Å, c = 7.2828 Å, β = 98.962°	$P2_1/c$[21]	
$BaGa_2O_4$	a = 5.393 Å, c = 8.974 Å	$P6_322$[23]	
	a = 18.6403 Å, c = 8.6801 Å	$P6_3$[24]	
$Ba_3Ga_2O_6$	a = 16.746 Å	$Pa\bar{3}$[22]	
$BaGa_{12}O_{19}$	a = 5.8140 Å, c = 23.038 Å	$P6_3/mmc$[25]	89−4674
	$Ga_2O_3-Ta_2O_5$ system		
$GaTaO_4$	a = 4.636 Å, c = 3.026 Å	$P4_2/mnm$[27]	15−0693
	a = 4.612 Å, b = 5.588 Å, c = 4.974 Å	$Pbcn$[26]	81−1197
	a = 4.60 Å, b = 5.57 Å, c = 4.97 Å, β = 90.40°	$P2/c$[27]	15−0691

deficient shifted hexagonal perovskite.[15] $BaTa_2O_6$ has three polymorphs: an orthorhombic phase (isostructural with $BaNb_2O_6$) stable up to 1150 °C,[16] a TTB $A_6B_{10}O_{30}$ type structure with a cell of ∼12 Å × ∼12 Å × ∼4 Å within ∼1150−1300 °C,[17] and a hexagonal phase above 1300 °C.[18] Within a 26−43 mol % BaO range in the $BaO-Ta_2O_5$ system, three TTB-related solid solutions form within 1275−1500 °C. In the 43−39 mol % BaO region, the TTB-related phase has a simple TTB $A_6B_{10}X_{30}$ unit cell, similar to the TTB-type $BaTa_2O_6$, and was formulated as $Ba_xTa_{(10-2x)/5}[Ta_{10}O_{30}]$ with Ba and the excess Ta distributed in a disordered manner over the square and pentagonal channels to avoid the oxygen vacancies in the octahedral network. In the 38−31 mol % BaO region, a doubled cell by $\sqrt{2}$ in the ab plane of the simple $A_6B_{10}O_{30}$ TTB cell forms in the TTB-related phase and the ordering of two [TaO] units per supercell within the pentagonal channels was proposed as the cause of the doubled cell, leading to a formula $Ba_xTa_{(14-2x)/5}[Ta_{22}O_{62}]$ for the $\sqrt{2}$-type solid solution. In the 30−26 mol % BaO region, a tripled cell by 3 times in the b axis of the simple TTB $A_6B_{10}O_{30}$ cell was observed in the TTB-type phase, and this triple-type solid solution was formulated as $Ba_xTa_{(18-2x)/5}[Ta_{34}O_{94}]$, which includes four ordered [TaO] units within pentagonal channels. These three TTB-related phases were also confirmed by Kolodiazhnyi et al.[19] in a phase equilibrium study of the $BaO-MgO-Ta_2O_5$ ternary system at 1450 °C.

The phase equilibrium diagram in the $BaO-Ga_2O_3$ system has been constructed by Kovba et al.[20] Four barium gallates, $Ba_4Ga_2O_7$, $Ba_3Ga_2O_6$, $BaGa_2O_4$, and $BaGa_{12}O_{19}$, form in this binary system. Kahlenberg[21] reported that $Ba_4Ga_2O_7$ has a monoclinic structure containing isolated Ga_2O_7 groups linked with Ba atoms from a single crystal X-ray diffraction study, contrary to the perovskite-related structure proposed by Kovba et al.[20] $Ba_3Ga_2O_6$ crystallizes a cubic structure consisting of isolated 12-membered rings formed by GaO_4 tetrahedra.[22] $BaGa_2O_4$ displays three low temperature and one high temperature polymorph with three-dimensional tetrahedral structures.[23,24] $BaGa_{12}O_{19}$ belongs to the magnetoplumbite structure family.[25] In the $Ga_2O_3-Ta_2O_5$ system, only $GaTaO_4$ forms, displaying one α-PbO_2 type polymorph at room temperature with orthorhombic[26] (ICDD PDF 15−0526) and monoclinic[27] (ICDD PDF 15−0691) modifications and one high temperature tetragonal rutile-type polymorph (ICDD PDF 15−0693).[27]

2. EXPERIMENTAL PROCEDURES

Approximately 85 polycrystalline samples for phase relationship investigation were synthesized from the mixed oxide route using $BaCO_3$ (99.9%), Ga_2O_3 (99.999%), and Ta_2O_5 (99.99%) as starting materials, which were dried at 400 °C before weighing. Starting materials according to different stoichiometries in 1.5 g batches were weighed and mixed with ethanol with an agate mortar and pestle for ∼10 min. The dried mixtures were calcined at 1200 °C for 24 h in alumina crucibles with heating and cooling rates of 5 °C/min, and the calcined mixtures were reground. This procedure was repeated to ensure that the equilibrations were reached, and no significant changes were observed in the powder X-ray diffraction (XRD) patterns.

The $Ba_6Ga_{21}TaO_{40}$ pellets for ac impedance spectroscopy measurement were made via the following process. $Ba_6Ga_{21}TaO_{40}$ powder was calcined at 1000 °C for 12 h and mixed with a polyvinylalcohol (PVA) binder and then pressed under ∼200 MPa of pressure into pellets with a 10 mm diameter and ∼3 mm thickness. The pellets were sintered at 1200 °C for 24 h and 1300 °C for 12 h followed by a final firing at 1350 °C for 12 h, leading to pellets with ∼80% relative density.

The phase assemblages of the products were studied using powder XRD at room temperature (RT), using a D8 ADVANCE powder diffractometer with Cu Kα radiation with 40 kV and 40 mA. The data for the structure analysis for $Ba_6Ga_{21}TaO_{40}$ were collected over a 2θ range from 10° to 110° at intervals of 0.02°. All of the powder XRD data were analyzed using Topas Academic software.[28]

dx.doi.org/10.1021/ic3008238 | Inorg. Chem. 2012, 51, 7788−7793

The structure solution for the $Ba_6Ga_{21}TaO_{40}$ was performed by the charge-flipping method, recently developed by Oszlányi and Sütő,[29−31] for phasing using the SUPERFLIP program[32] implemented in the JANA2006[33] software package combined with the Le Bail method[34] for decomposing the powder diffraction. The structure solution led to all of the metal sites and partial oxygen sites, which were refined by the Rietveld method[35] using Topas Academic software on the powder XRD data. The remaining two oxygen sites were located through difference Fourier map calculation. Minimum interatomic distance constraints of O−O (2.4 Å), Ga/Ta−O (1.7 Å), and Ba−O (2.4 Å) were applied during the refinement of the partial structure before successfully locating the missing two oxygen positions and then were removed for the refinement of the complete structure, where no rigid bodies or individual bond length and angle restraints were used for the tetrahedra and octahedra. Bond valence sums (BVSs) were calculated by Brown and Altermatt's method.[36]

Ac impedance spectroscopy measurement was carried out by using a Solartron1260A impedance/gain-phase analyzer over 10^{-1} to 10^7 Hz from room temperature to 1000 °C. Prior to the IS measurement, the pellet was coated with platinum paste and fired at 800 °C for 30 min to burn out the organic components to form electrodes. For calculation of dielectric permittivity for the material itself, the measured capacitance from the impedance data was corrected by subtracting the blank contribution arising from the sample holder and connection cables, which was measured on an open circuit without the pellet.

3. RESULTS AND DISCUSSION

3.1. Phase Relationships in the $BaO−Ga_2O_3−Ta_2O_5$ System. Figure 1 shows the $BaO−Ga_2O_3−Ta_2O_5$ phase

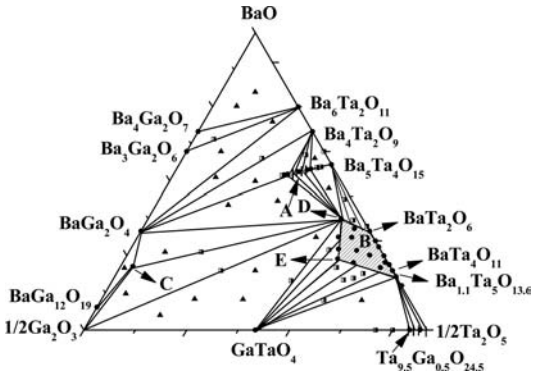

Figure 1. Phase diagram of the $BaO−Ga_2O_3−Ta_2O_5$ ternary system at 1200 °C. A, B, C, D, and E denote the hexagonal perovskite solid solution 8H-BGT, the TTB-related solid solution, $Ba_6Ga_{21}TaO_{40}$, $Ba_6GaTa_9O_{30}$, and $Ba_{1.58}Ga_{0.92}Ta_{4.08}O_{13.16}$, respectively. The trapezoid-shaped ternary TTB-related solid solution region is marked by hatching. The half-filled square ◨ and filled triangle ▲ symbols represent that the associated compositions are located in two-phase and three-phase regions, respectively.

diagram at 1200 °C. The phase diagram is divided into 14 three-phase regions, five two-phase regions, and an $A_6B_{10}O_{30}$ TTB-related solid solution region and contains the 8H-BGT solid solution and the ternary phase $Ba_6Ga_{21}TaO_{40}$. The compositions attempted and phases assemblages in the final products for the $BaO−Ga_2O_3−Ta_2O_5$ ternary system are summarized in Table S1, Supporting Information (SI).

In the $BaO−Ta_2O_5$ subsystem, $Ba_6Ta_2O_{11}$, $Ba_4Ta_2O_9$, $Ba_5Ta_4O_{15}$, and $BaTa_2O_6$ line phases were confirmed, and the formation of $Ba_3Ta_2O_8$ was not observed in this study. A single $A_6B_{10}O_{30}$ TTB-related phase was observed in samples within the 50−30.5 mol % BaO range, which compares to the 43−26 mol % BaO range of the TTB-related solid solution at 1275−1500 °C reported by Vanderah et al.[12]

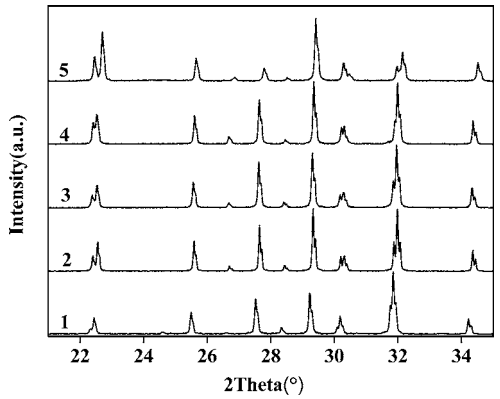

Figure 2. XRD patterns of the selected samples in the TTB-related solid solution. Patterns 1−5 correspond to samples $Ba_6GaTa_9O_{30}$, $BaTa_2O_6$, $Ba_{2.27}Ga_{0.45}Ta_{4.55}O_{14.32}$, $Ba_{1.58}Ga_{0.92}Ta_{4.08}O_{13.16}$, and $Ba_{1.1}Ta_5O_{13.6}$, respectively.

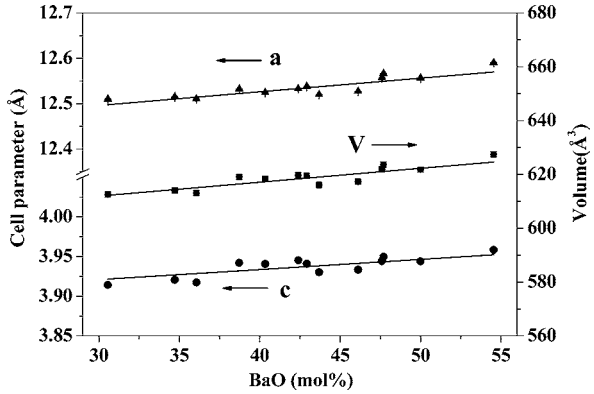

Figure 3. Cell parameters for the TTB-related solid solution.

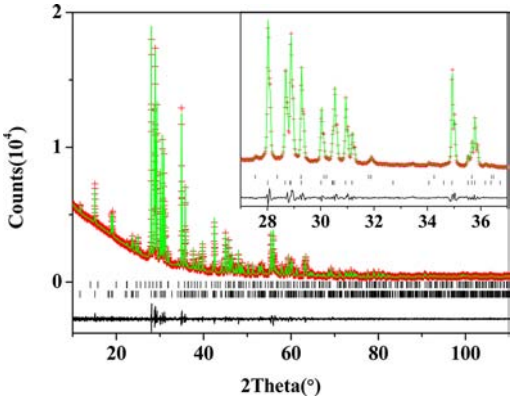

Figure 4. Rietveld refinement of XRD data for $Ba_6Ga_{21}TaO_{40}$. The two rows of vertical tick marks from bottom to top correspond to the Bragg diffraction positions of the major phase $Ba_6Ga_{21}TaO_{40}$ and the minor phase TTB $Ba_6GaTa_9O_{30}$, respectively. The inset enlarges the fit over the 27−37° 2Θ range.

As demonstrated in the studies of the $BaO−TiO_2−Ta_2O_5$ and $BaO−MgO−Ta_2O_5$ systems, the TTB-related phase in the $BaO−Ta_2O_5$ system can dissolve up to 12 mol % TiO_2 and 1.5−2 mol % MgO, respectively. In this study, the TTB-related phase extended into the ternary region by dissolving up to 11 mol % Ga_2O_3, which formed a trapezoid-shaped TTB-related

dx.doi.org/10.1021/ic3008238 | Inorg. Chem. 2012, 51, 7788−7793

Table 2. Final Refined Structural Parameters for $Ba_6Ga_{21}TaO_{40}$[a]

atom	site	x	y	z	occupancy	B_{iso} (Å^2)	BVS[b]
Ba1	4*i*	0.7194(1)	0	0.2431(4)	1	1.17(5)	1.86
Ba2	2*c*	0	0	0.5	1	1.89(8)	1.78
Ga1	2*d*	0.5	0	0.5	0.709(5)	1.5(1)	3.29
Ta1	2*d*	0.5	0	0.5	0.291(5)	1.5(1)	5.50
Ga2	4*g*	0.5	0.1372(3)	0	0.895(5)	1.69(7)	2.77
Ta2	4*g*	0.5	0.1372(3)	0	0.105(5)	1.69(7)	4.63
Ga3	8*j*	0.3623(2)	0.2139(2)	0.3338(6)	1	1.43(7)	2.90
Ga4	8*j*	0.3533(2)	0.3626(2)	−0.1551(7)	1	1.44(6)	3.20
O1	8*i*	0.0850(7)	0.2497(9)	−0.059(2)	1	1.3(1)	2.00
O2	4*i*	−0.0618(7)	0.5	0.112(2)	1	1.3(1)	1.99
O3	4*j*	0.097(1)	0	0.016(3)	1	1.3(1)	1.93
O4	8*j*	0.3577(7)	0.6491(4)	0.497(1)	1	1.3(1)	2.03
O5	8*j*	0.4270(7)	0.8860(5)	0.608(2)	1	1.3(1)	1.96
O6	8*j*	0.2614(5)	0.1364(9)	0.179(2)	1	1.3(1)	1.99

[a]Space group $C2/m$, $Z = 1$, $a = 15.9130(2)$ Å, $b = 11.7309(1)$ Å, $c = 5.13593(6)$ Å, $\beta = 107.7893(9)°$, and $V = 912.90(2)$ Å^3; $R_{wp} \sim 3.53\%$ Rp ∼ 2.36%, $R_B \sim 1.43\%$. The atomic displacement factors B_{iso} for all the oxygen sites are constrained to be identical. [b]The Ga/Ta occupancies on the mixed octahedral (Ga/Ta)1 and (Ga/Ta)2 sites are considered in the BVS calculation for the oxygen sites.

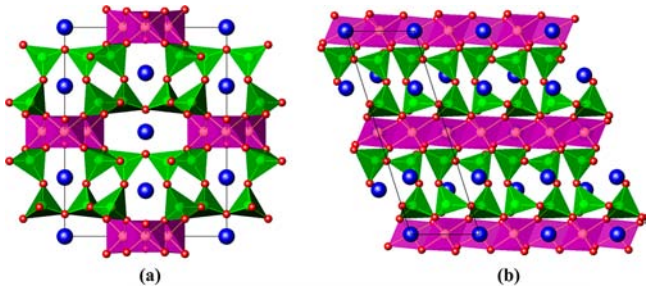

Figure 5. Projections along the *c* axis (a) and the *b* axis (b) of the structure of $Ba_6Ga_{21}TaO_{40}$. The blue and red spheres represent Ba and oxygen atoms, respectively. The GaO_4 tetrahedra and $(Ga/Ta)O_6$ octahedra are plotted in green and pink, respectively.

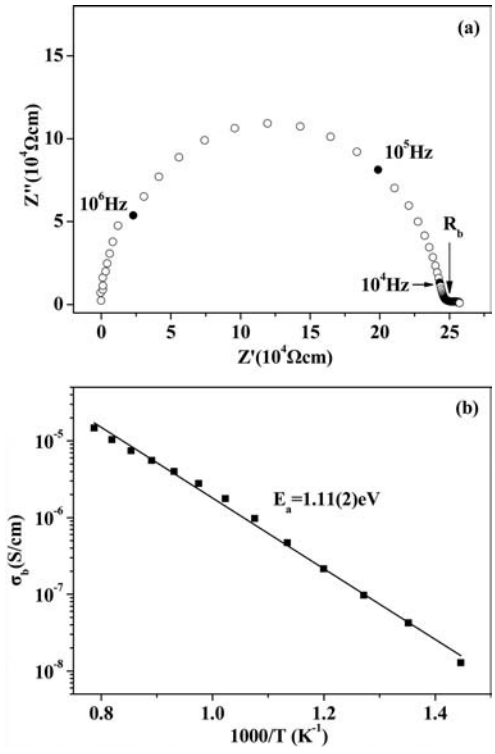

Figure 6. Complex impedance plot recorded at 800 °C (a) and Arrhenius plot of the bulk conductivity (b) for the $Ba_6Ga_{21}TaO_{40}$ pellet. R_b denotes bulk resistivity, and the selected frequencies for the data marked by the filled circles are shown in (a).

solid solution region defined by the four points at $BaTa_2O_6$, $Ba_{1.1}Ta_5O_{13.6}$, $Ba_{1.58}Ga_{0.92}Ta_{4.08}O_{13.16}$, and $Ba_6GaTa_9O_{30}$. The XRD patterns of the selected samples of this solid solution are shown in Figure 2. In contrast with the three TTB-related solid solutions, all of the XRD patterns of the TTB-related phases can be indexed with the simple $A_6B_{10}X_{30}$ cell and did not show strong evidence of $\sqrt{2}$-type or tripled TTB superstructures. The cell parameters as functions of BaO mol % are shown in Figure 3, which exhibit trends of higher BaO mol % and larger cell parameters. In the trapezoid-shaped TTB-related solid solution region, the tunnels in the TTB structure are free of Ta atoms in the materials along the $Ba_6GaTa_9O_{30}$–$BaTa_2O_6$ line, and the remaining materials may contain disordered Ta in the tunnels or [TaO] units in the pentagonal tunnels, as suggested by Vanderah et al.[12] Determining the Ta/O distribution over the tunnels in the TTB structure for this TTB-related solid solution in the $BaO–Ga_2O_3–Ta_2O_5$ system awaits further structural analysis using both X-ray and neutron diffraction data, which is not in the scope of this study.

In the $Ga_2O_3–Ta_2O_5$ subsystem, the $GaTaO_4$ phase was confirmed and Ta_2O_5 dissolved up to 5 mol % Ga_2O_3, forming a solid solution $Ta_{2-x}Ga_xO_{5-2x}$ in a narrow range of $0 \le x \le 0.1$. In the $BaO–Ga_2O_3$ subsystem, formations of $Ba_3Ga_2O_6$, $Ba_4Ga_2O_7$, $BaGa_2O_4$, and $BaGa_{12}O_{19}$ were observed at 1200 °C. In the BaO-rich three phase region above the $Ba_4Ga_2O_7$–$Ba_6Ta_2O_{11}$ line, the samples were found unstable at room temperature in the air, turning into barium carbonate and $Ba(OH)_2·H_2O$ phases plus significant amorphous materials, as detected by XRD, which could be ascribed to the reaction of the BaO-rich phases and BaO with the moisture or CO_2. The instability for the BaO-rich region was noticed by Kolodiazhnyi et al.[19] in the $BaO–MgO–Ta_2O_5$ ternary system and Kovba et al.[20] in the $BaO–Ga_2O_3$ binary system.

Apart from the TTB-related solid solution in the $BaO–Ga_2O_3–Ta_2O_5$ ternary system, the ternary 8H-BGT solid solution formed, and its limits obtained at 1200 °C agree well with our previous results obtained at 1450 °C.[9] The 8H-BGT has a twinned eight-layer hexagonal perovskite structure,

dx.doi.org/10.1021/ic3008238 | Inorg. Chem. 2012, 51, 7788–7793

consisting of cubic and hexagonal BaO_3 layers stacked in a sequence of $(ccch)_2$ in space group $P6_3cm$ and exhibits partial cation and vacancy ordering in the face-sharing octahedral sites, leading to expanded cell parameters by $\sqrt{3}$ in the *ab* plane with respect to those in the simple eight-layer hexagonal perovskite cell. The 8H-BGT structure details have been published in ref 9. The formation of the $Ba_6Ga_{21}TaO_{40}$ ternary phase was also confirmed, and its structure is described in the following section.

3.2. Structure and Impedance Data of $Ba_6Ga_{21}TaO_{40}$. The XRD pattern for $Ba_6Ga_{21}TaO_{40}$ had been indexed in a monoclinic cell of a_I = 15.1649 Å, b_I = 11.7315 Å, c_I = 5.1365 Å, and β_I = 91.0180° in space group $I2/m$[10] (ICDD PDF 47−0535). In this study, the standard C-centered cell in space group $C2/m$ ($a = -a_I - c_I$, $b = -b_I$; $c = c_I$) was employed for $Ba_6Ga_{21}TaO_{40}$ and the refined C-centered cell parameters are a = 15.9130(2) Å, b = 11.7309(1) Å, c = 5.13593(6) Å, and β = 107.7893(9)°. The structural model of $Ba_6Ga_{21}TaO_{40}$ consists of 12 crystallographically distinct atoms: two Ba sites, four sites for Ga and Ta, and six oxygen sites. Refinement showed that among the sites for Ga and Ta, two 8*j* sites are tetrahedral Ga sites, and the remaining two sites (2*d* and 4*g*) are mixed octahedral Ga/Ta sites. The TTB $Ba_6GaTa_9O_{30}$ (1.53(5) wt%) was observed as a minor second phase in the sample and was added in the refinement, which converged to $R_{wp} \sim 3.53\%$ and $R_B \sim 1.43\%$. The Rietveld plot for $Ba_6Ga_{21}TaO_{40}$ is shown in Figure 4. Table 2 lists the final refined structural parameters for $Ba_6Ga_{21}TaO_{40}$. The bond lengths and angles for $Ba_6Ga_{21}TaO_{40}$ are given in Tables S2 and S3, respectively in the SI.

The structure of $Ba_6Ga_{21}TaO_{40}$, shown in Figure 5, displays three-dimensional mixed GaO_4 tetrahedral and GaO_6/TaO_6 octahedral framework. Along the *c* axis, the $(Ga/Ta)O_6$ octahedra form one-dimensional sheets via sharing the edges. In GaO_4 tetrahedra, all of the oxygen atoms are bridging oxygen. The GaO_4 tetrahedra form a 2D corner-sharing tetrahedral block, linked with the $(Ga/Ta)O_6$ octahedral sheets via sharing corners. The linkage of tetrahedral blocks and octahedral sheets forms 4/5/6-fold tunnels along the *c* axis, among which the Ba atoms occupy the 5/6-fold tunnels as chains of cations, leaving the 4-fold tunnels unoccupied. The coexistence of GaO_4 and GaO_6 polyhedra in $Ba_6Ga_{21}TaO_{40}$ is similar to the mixed GaO_n polyhedra observed in the magnetoplumbite-type $BaGa_{12}O_{19}$ (mixed GaO_6 and GaO_5)[25] and the recently identified interstitial oxygen conducting melilite $La_{1+x}A_{1-x}Ga_3O_{7+0.5x}$ (A = Sr, Ca) (mixed GaO_4 and GaO_5).[37,38] $Ba_6Ga_{21}TaO_{40}$ represents a structure type with a general formula $A_6B'_6B''_{16}O_{40}$, where B cations have a mixed polyhedral $B''O_4$ and $B'O_6$ environment and the large A cations sit in the 1D pentagonal and hexagonal tunnels formed by the 3D mixed polyhedral framework.

Figure 6a shows a typical complex impedance plot measured at 800 °C, which comprises a large and a small semicircular arc. The large semicircular arc could be modeled with parallel resistor (R) and capacitor (C) elements. The R was estimated as the intercept at low frequency of the large semicircular arc, and the C, estimated from the equation $\omega RC = 1$ (ω is angular frequency, $2\pi f_{max}$, where f_{max} is the frequency corresponding to the maximum Z″) is ∼2.5 pF/cm, consistent with the bulk response.[39] The small semicircular arc shows large capacitance with a magnitude of 10^{-11} to 10^{-8} F/cm over the 10^2 to 10^{-1} Hz frequency range, ascribed to the grain boundary response. The $Ba_6Ga_{21}TaO_{40}$ pellet shows insulator behavior: the bulk conductivity is in the range 10^{-8} to 10^{-5} S/cm over the 400−1000 °C range with an activation energy E_a of 1.11(2) eV (Figure 6b). The dielectric permittivity ε_r at 1 MHz, calculated from the capacitance corrected by subtracting the blank capacitance arising from the sample holder and connection cables, is ∼13 at room temperature. The temperature coefficient of dielectric permittivity is ∼6185 ppm/ °C from room temperature to 1000 °C. As shown in Figure 6a, the bulk response dominates the impedance data in the high frequency region >10^3 Hz; therefore, the permittivity in the high frequency region is mainly from the bulk contribution. Given the low pellet density (∼80%), the bulk permittivity and conductivity from the impedance measurement would be smaller than those for the well-sintered pellet if available.

4. CONCLUSIONS

Phase relationships in the $BaO-Ga_2O_3-Ta_2O_5$ ternary system at 1200 °C were determined on the basis of the powder XRD data. The $A_6B_{10}O_{30}$ TTB-related solution in the $BaO-Ta_2O_5$ subsystem dissolved up to ∼11 mol % Ga_2O_3, forming a ternary trapezoid-shaped TTB-related solid solution region in the $BaO-Ga_2O_3-Ta_2O_5$ system. Two ternary phases $Ba_6Ga_{21}TaO_{40}$ and eight-layer twinned hexagonal perovskite solid solution $Ba_8Ga_{4-x}Ta_{4+0.6x}O_{24}$ were confirmed in the $BaO-Ga_2O_3-Ta_2O_5$ system. $Ba_6Ga_{21}TaO_{40}$ crystallized in a monoclinic $C2/m$ structure consisting of a 3D mixed GaO_4 tetrahedral and GaO_6/TaO_6 octahedral framework with mixed 5/6-fold tunnels accommodating the Ba cations along the *c* axis, representing a structure type with a general formula $A_6B'_6B''_{16}O_{40}$, where the corner-shared $B''O_4$ tetrahedral layers link with the edge-shared $B'O_6$ octahedral sheets to form a 3D framework with 1D pentagonal and hexagonal tunnels to accommodate the large A cations.

■ ASSOCIATED CONTENT

Ⓢ Supporting Information

Composition attempted and phase assemblages in the final products in the $BaO-Ga_2O_3-Ta_2O_5$ ternary system, bond lengths and bond angles of Ga−O−Ga in $Ba_6Ga_{21}TaO_{40}$, and a crystallographic information file in CIF format for $Ba_6Ga_{21}TaO_{40}$. This material is available free of charge via the Internet at http://pubs.acs.org.

■ AUTHOR INFORMATION

Corresponding Author

*E-mail: kuangxj@mail.sysu.edu.cn.

Notes

The authors declare no competing financial interest.

■ ACKNOWLEDGMENTS

The Guangdong Natural Science Foundation is acknowledged for the financial support (S2011010001310). We thank Xiaolan Yu (Sun Yat-Sen University) for assistance on the measurement of XRD.

■ REFERENCES

(1) Reaney, I. M.; Iddles, D. *J. Am. Chem. Soc.* **2006**, *89*, 2063−2072.
(2) Chi, E. O.; Gandini, A.; Ok, K. M.; Lei, Z.; Halasyamani, P. S. *Chem. Mater.* **2004**, *16*, 3616−3622.
(3) Hughes, H.; Iddles, D. M.; Reaney, I. M. *Appl. Phys. Lett.* **2001**, *79*, 2952−2954.
(4) Lufaso, M. W. *Chem. Mater.* **2004**, *16*, 2148−2156.

(5) Moussa, S. M.; Claridge, J. B.; Rosseinsky, M. J.; Clarke, S.; Ibberson, R. M.; Price, T.; Iddles, D. M.; Sinclair, D. C. *Appl. Phys. Lett.* **2003**, *82*, 4537−4539.
(6) Kan, A.; Ogawa, H.; Yokoi, A.; Ohsato, H. *Jpn. J. Appl. Phys.* **2006**, *45*, 7494−7498.
(7) Kawaguchi, S.; Ogawa, H.; Kan, A.; Ishihara, S. *J. Eur. Ceram. Soc.* **2006**, *26*, 2045−2049.
(8) Fang, L.; Li, C. C.; Peng, X. Y.; Hu, C. Z.; Wu, B. L.; Zhou, H. F. *J. Am. Ceram. Soc.* **2010**, *93*, 1229−1231.
(9) Cao, J.; Kuang, X.; Allix, M.; Dickinson, C.; Claridge, J. B.; Rosseinsky, M. J.; Iddles, D. M.; Su, Q. *Chem. Mater.* **2011**, *23*, 5058−5067.
(10) Kaminskii, A. A.; Mill, B. V.; Belokoneva, E. L.; Butashin, A. V.; Sarkisov, S. E.; Kurbanov, K.; Khodzhabagyan, G. G. *Izv. Akad. Nauk SSSR, Neorg. Mater.* **1986**, *22*, 1869−1873.
(11) Kovba, L. M.; Lykova, L. N.; Paromova, M. V.; Lopato, L. M.; Shevchenko, A. V. *Russ. J. Inorg. Chem.* **1977**, *20*, 2845−2847.
(12) Vanderah, T. A.; Roth, R. S.; Siegrist, T.; Febo, W.; Loezos, J. M.; Wong-Ng, W. *Solid State Sci.* **2003**, *5*, 149−164.
(13) Brixner, L. H. *J. Am. Chem. Soc.* **1958**, *80*, 3214−3215.
(14) Ling, C. D.; Avdeev, M.; Kharton, V. V.; Yaremchenko, A. A.; Macquart, R. B.; Hoelzel, M. *Chem. Mater.* **2010**, *22*, 532−540.
(15) Shannon, J.; Katz, L. *Acta Crystallogr., Sect. B* **1970**, *26*, 102−105.
(16) Layden, G. K. *Mater. Res. Bull.* **1967**, *2*, 533−539.
(17) Galasso, F.; Katz, L.; Ward, R. *J. Am. Chem. Soc.* **1959**, *81*, 5898−5899.
(18) Mumme, W. G.; Grey, I. E.; Roth, R. S.; Vanderah, T. A. *J. Solid State Chem.* **2007**, *180*, 2429−2436.
(19) Kolodiazhnyi, T.; Belik, A. A.; Ozawa, T. C.; Takayama-Muromachi, E. *J. Mater. Chem.* **2009**, *19*, 8212−8215.
(20) Kovba, L. M.; Lykova, L. N.; Kobzareva, V. P.; Lopato, L. M. *Russ. J. Inorg. Chem.* **1975**, *20*, 1098−1100.
(21) Kahlenberg, V. *Z. Anorg. Allg. Chem.* **2001**, *32*, 2386−2390.
(22) Kahlenberg, V. *Cryst. Res. Technol.* **2001**, *36*, 316−329.
(23) Kahlenberg, V.; Weidentthaler, C. *Solid State Sci.* **2002**, *4*, 963−968.
(24) Kahlenberg, V.; Fischer, R. X.; Parise, J. B. *J. Solid State Chem.* **2000**, *154*, 612−618.
(25) Wagner, T. R. *J. Solid State Chem.* **1998**, *136*, 120−124.
(26) Harneit, O.; Müller-Buschbaum, H. *J. Alloys Compd.* **1993**, *194*, 101−103.
(27) Plotkin, S. S.; Plyushchev, V. E. *Powder Metall. Met. Ceram.* **1972**, *11*, 137−140.
(28) Coelho, A. A. *TOPAS Academic V4*; Coelho Software: Brisbane, Australia, 2005.
(29) Baerlocher, C.; McCusker, L. B.; Palatinus, L. *Z. Kristallogr.* **2007**, *222*, 47−53.
(30) Wu, J. S.; Leinenweber, K.; Spence, J. C. H.; O'Keeffe, M. *Nat. Mater.* **2006**, *5*, 647−652.
(31) Oszlanyi, G.; Suto, A. *Acta Crystallogr., Sect. A.* **2004**, *60*, 134−141.
(32) Palatinus, L.; Chapuis, G. *J. Appl. Crystallogr.* **2007**, *40*, 786−790.
(33) Petricek, V.; Dusek, M.; Palatinus, L. *Jana2006, The Crystallographic Computing System*; Institute of Physics: Praha, Czech Republic, 2006.
(34) Le Bail, A.; Duroy, H.; Fourquet, J. L. *Mater. Res. Bull.* **1988**, *23*, 447−452452.
(35) Rietveld, H. M. *J. Appl. Crystallogr.* **1969**, *2*, 65−7171.
(36) Brown, I. D.; Altermatt, D. *Acta Crystallogr., Sect. B* **1985**, *41*, 244−247.
(37) Kuang, X. J.; Green, M. A.; Niu, H.; Zajdel, P.; Dickinson, C.; Claridge, J. B.; Jantsky, L.; Rosseinsky, M. J. *Nat. Mater.* **2008**, *7*, 498−504.
(38) Li, M. R.; Kuang, X. J.; Chong, S. Y.; Xu, Z. L.; Thomas, C. I.; Niu, H. J.; Claridge, J. B.; Rosseinsky, M. J. *Angew. Chem., Int. Ed.* **2010**, *49*, 2362−2366.
(39) Irvine, J. T. S.; Sinclair, D. C.; West, A. R. *Adv. Mater.* **1990**, *2*, 132−138.